High-Pressure Studies of Radical−Solvent Molecule Interactions in the CCl_3 and Bromine Combination Reactions of CCl_3

Kawon Oum, Klaus Luther,* and Jürgen Troe

Institut für Physikalische Chemie, Universität Göttingen, Tammannstrasse 6, D-37077 Göttingen, Germany

Received: November 14, 2003; In Final Form: February 11, 2004

The combination reactions $CCl_3 + CCl_3$ (+ M) → C_2Cl_6 (+ M) and $CCl_3 + Br$ (+ M) → CCl_3Br (+ M) (with rate constants of k_1 and k_2, respectively) were studied at temperatures of 250 and 300 K over the pressure range of 0.01−1000 bar. Helium, argon, xenon, N_2, CO_2, and SF_6 were used as bath gases. CCl_3 radicals were generated via the photolysis of CCl_3Br at 248 nm, and their absorption was monitored at 223.5 nm. The limiting "high-pressure" rate constants within the energy-transfer mechanism were determined, independent of density and the choice of the bath gas, over the pressure range of 1−10 bar, to be $k_{1,\infty}(T) = (1.0 \pm 0.2) \times 10^{-11}$ $(T/300\ \mathrm{K})^{-0.17}$ cm^3 molecule^{-1} s^{-1} and $k_{2,\infty}(T) = (2.0 \pm 0.2) \times 10^{-11}$ $(T/300\ \mathrm{K})^{-0.13}$ cm^3 molecule^{-1} s^{-1}. In the helium, N_2, and argon bath gases, at pressures above ∼40 bar, the reactions became increasingly faster when the pressure was further raised until they finally started to slow at densities where diffusion-controlled kinetics dominates. This is the first detailed report of such a peculiar density dependence of combination rate constants for larger radicals with five or eight atoms. Possible origins of these pressure effects, such as the influence of the radical-complex mechanism and the density dependence of electronic quenching, are discussed.

Introduction

Interactions between reagents and bath gases or solvents can influence chemical reaction dynamics in various ways, ranging from molecular transport to intermolecular energy transfer and the formation of radical−bath gas complexes. Originally postulated in the "chaperon mechanism" of atom recombination,[1,2] radical−bath-gas complexes have found increasing interest recently, e.g., in studies of the reactions in supercritical solvents[3] and in discussions about the role of weakly bound complexes even in atmospheric chemistry.[4−6] Studies of pressure and temperature-dependent rate constants of atom and radical combination reactions can provide a useful access to the understanding of such intermolecular interactions in the gas-to-liquid transition range. This is the issue of the present article.

Traditionally, radical combination reactions are interpreted within the energy-transfer (ET) mechanism with association, dissociation, and collisional-energy transfer steps,

$$A + A \rightleftarrows A_2^* \qquad (k_a, k_{-a}) \qquad \text{(Ia)}$$

$$A_2^* + M \rightarrow A_2 + M \qquad (k_b) \qquad \text{(Ib)}$$

resulting in characteristic limiting low- and high-pressure rate constants (k_0^{ET} and k_∞^{ET}) and an intermediate fall-off regime. An alternative reaction path would be the radical-complex (RC) or chaperon mechanism, which may have an important role, depending on the strength of interaction between A and M:

$$A + M \rightleftarrows AM \qquad (k_c, k_{-c}, K_{eq}) \qquad \text{(IIa)}$$

$$A + AM \rightarrow A_2 + M \qquad (k_d) \qquad \text{(IIb)}$$

$$AM + AM \rightarrow A_2 + 2M \qquad (k_e) \qquad \text{(IIc)}$$

In addition, one should be aware of the density dependence of collisional electronic (CE) quenching, which affects the probabilities of spin interconversion in radical pairs and can have some role in the kinetics of radical combination.

$$^2A\cdot + {}^2A\cdot \rightleftarrows {}^3[A...A] \leftrightarrow (+M) \rightleftarrows {}^1[A...A] \rightarrow {}^1A_2 \qquad \text{(III)}$$

There have been several experimental studies on combination reactions of atoms and small radicals (see, for example, Oum et al.,[3] Hippler and co-workers,[4,7−10] and Stark[11]), in which indications for a radical−complex (RC) mechanism were found; however, a separation of the contributions from the various mechanisms was always difficult. The present study provides another example of a new experimental strategy[3] to separate these mechanisms. We choose systems in which the limiting high-pressure rate constant of the ET mechanism is attained at relatively low pressures under conditions where the RC mechanism is not yet expected to be important. We then increase the pressure up to conditions where the RC mechanism may become visible. We report here a study of the combination reactions of CCl_3 radicals with themselves and with bromine over a very wide pressure range of 0.01−1000 bar at temperatures of 250 and 300 K:

$$CCl_3 + CCl_3\,(+M) \rightarrow C_2Cl_6 \quad (+M) \qquad (k_1) \qquad (1)$$

$$CCl_3 + Br\,(+M) \rightarrow CCl_3Br \quad (+M) \qquad (k_2) \qquad (2)$$

Both reactions approach the limiting high-pressure rate constant k_∞^{ET} below ∼1−10 bar, and this high-pressure range is experimentally established over a certain pressure range. With further increases in pressure (beyond ∼40 bar) and before the onset of diffusion control, a pressure-independent and bath-gas-inde-

* Author to whom correspondence should be addressed. E-mail: kluther@gwdg.de.

10.1021/jp0374861 CCC: $27.50 © 2004 American Chemical Society
Published on Web 03/17/2004

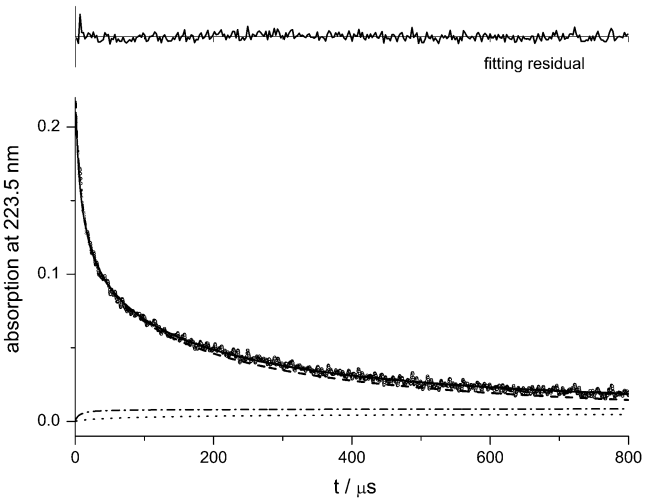

Figure 1. Absorption signal at 223.5 nm, recorded after photolysis of CCl_3Br ($[CCl_3]_0 = 2.7 \times 10^{15}$ molecule cm^{-3}, $p(N_2) = 698$ bar, $T = 300$ K; signal averaged over 100 laser shots). Legend is as follows: (− − −) fitted profile of CCl_3, (· · ·) fitted profile for C_2Cl_6, (− · −) fitted profile of CCl_3Br, and (—) complete absorption signal. Residual of the fitting procedure is shown at the top of the figure.

pendent high-pressure limit is no longer observed. Instead, an increase of the rate constants appears. These observations are direct experimental indications for dynamical phenomena such as the RC mechanism or pressure-dependent efficiencies of CE quenching which may be superimposed on the simple fall-off curve of the usual ET mechanism.

Experimental Section

Our high-pressure flow cell has been described in detail elsewhere,[11−13] and only the main features are given here. Briefly, CCl_3 radicals in the high-pressure cell were formed by the laser photolysis of CCl_3Br at 248 nm:

$$CCl_3Br + h\nu\ (248\ nm) \rightarrow CCl_3 + Br \qquad (3)$$

The UV absorption at 223.5 nm over a path length of 10 cm was used to monitor the temporal loss of the radicals by reactions. Mixtures of the gaseous precursor CCl_3Br and the bath gas were compressed in an oil-free diaphragm compressor (Nova Swiss, model 5542321), and then flowed through the high-pressure cell. The gas flow was controlled by flow meters (Tylan models FM361 and FM362) at rates such that the observation volume was filled with a fresh reagent-bath gas mixture after each laser pulse. Total pressures were measured with high-pressure manometers (Burster, model 8201). Low temperatures were generated by flowing liquid nitrogen through a cooling copper tube covering the outside of the cell. Two platinum resistance thermometers were directly attached to the front and back of the cell and controlled the temperature. For experiments <1 bar, a glass flow cell was used in a separate setup (path length of 52 cm and optical diameter of 3 cm). CCl_3Br (Aldrich, 99.9%) was purified in a pump−thaw−freezing cycle before use. All other bath gases were of a purity better than 99.998% (Messer−Griesheim), and residual impurities in the bath gases were further removed using commercial gas cleaning adsorbers (Oxisorb, Messer−Griesheim) and dust filters.

Results

Figure 1 shows a typical absorption signal at 223.5 nm recorded after 248-nm laser photolysis of the mixture of

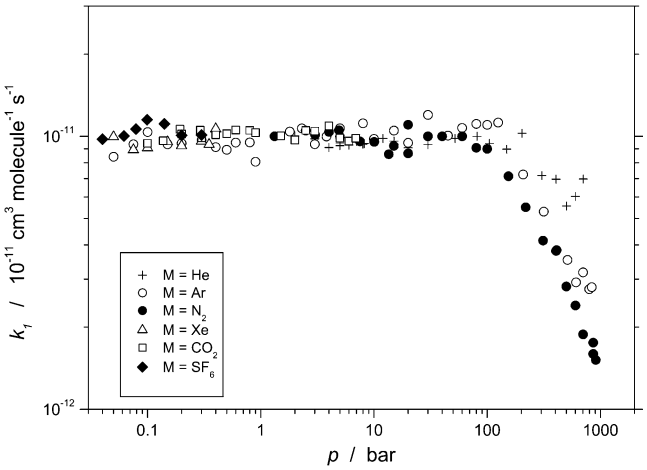

Figure 2. Combination rate constants of $CCl_3 + CCl_3$ (+ M) → C_2Cl_6 (+ M) (reaction 1) at 300 K; measurements in this work were made in the bath gases helium, argon, xenon, N_2, CO_2, and SF_6.

precursor (CCl_3Br) and bath gas (698 bar N_2, in this case) at 300 K. The signal corresponds to the decreasing concentration of CCl_3 radicals due to reactions 1 and 2. Reactions 4 and 5 also have a role:

$$Br + Br\ (+ M) \rightarrow Br_2\ (+ M) \qquad (4)$$

$$CCl_3 + Br_2 \rightarrow CCl_3Br + Br \qquad (5)$$

Signal analysis was performed with the absorption cross sections for CCl_3 ($\sigma = 8.8 \times 10^{-18}$ cm^2 $molecule^{-1}$),[14,15] C_2Cl_6 ($\sigma \approx 7 \times 10^{-19}$ cm^2 $molecule^{-1}$), and CCl_3Br ($\sigma \approx 6 \times 10^{-19}$ cm^2 $molecule^{-1}$). Reactions of the primary products bromine and CCl_3 with the precursor molecules need not be included: Br + CCl_3Br → Br_2 + CCl_3 (reaction −5) with $k_{-5} \approx 7 \times 10^{-16}$ cm^3 $molecule^{-1}$ s^{-1} at 420−455 K[16,17] is too slow, and CCl_3 + CCl_3Br → C_2Cl_6 + Br is most probably slower than CH_3 + CCl_3Br → CH_3Br + CCl_3 ($k \approx 5 \times 10^{-15}$ cm^3 $molecule^{-1}$ s^{-1} at 363 K),[18] but it would not even interfere if this assumption is not strictly fulfilled. The rate constants of reaction 4 have been previously measured in our group, up to 7000 bar in helium, argon, N_2, and CO_2.[19] The bimolecular rate constant of reaction 5 was calculated in a manner similar to that determined in the work by Hudgens et al.[20] With careful systematic modeling,[21] it was possible to evaluate the individual rate constants of reactions 1 and 2 because of the discriminating influence of reaction 4 under our conditions. Typical concentrations in our study were $[CCl_3]_0 = (1-10) \times 10^{15}$ molecule cm^{-3}.

Our results on the pressure dependence of k_1 obtained at temperatures near 300 K for the bath gases helium, argon, xenon, N_2, CO_2, and SF_6 are given in Table 1 and Figure 2. The limiting "high-pressure" rate constant of the ET mechanism was determined to be $k_{1,\infty}^{ET} = (1.0 \pm 0.2) \times 10^{-11}$ cm^3 $molecule^{-1}$ s^{-1}, independent of the bath gas and considering all data points between 10 and 40 bar. Indications of a further increase of k_1 near 40−100 bar in N_2 and argon, before diffusion control is established, are less visible than that for k_2, such as that shown in Figure 3, but are revealed at closer analysis (see below). The observed monotonic decrease of the rate constants starting at pressures of N_2 and argon near 100 bar corresponds to a smooth transition into the regime of diffusion-controlled kinetics such as that expected for these densities.

Results on the pressure dependence of k_2 for the bath gases helium, argon, xenon, N_2, CO_2, and SF_6 are given in Figure 3 and Table 1. Observations of k_2 in the flat portion near 10−40

TABLE 1: Pseudo-Second-Order Rate Constants for the Combination Reaction $CCl_3 + CCl_3$ (+ M) → C_2Cl_6 (+ M) (k_1) and $CCl_3 + Br$ (+M) → CCl_3Br (+M) (k_2) at 300 and 250 K

N_2 Data at 300 K

$p(N_2)^a$	$[N_2]^b$	$k_1{}^c$	$k_2{}^c$	$p(N_2)^a$	$[N_2]^b$	$k_1{}^c$	$k_2{}^c$	$p(N_2)^a$	$[N_2]^b$	$k_1{}^c$	$k_2{}^c$
1.32	3.19×10^{19}	1.07 ± 0.05	1.86 ± 0.11	20.00	4.83×10^{20}	1.01 ± 0.04	2.56 ± 0.10	311.00	6.51×10^{21}	0.42 ± 0.01	4.48 ± 0.10
3.01	7.27×10^{19}	1.01 ± 0.05	1.72 ± 0.10	30.00	7.24×10^{20}	1.00 ± 0.03	2.29 ± 0.09	406.00	7.81×10^{21}	0.38 ± 0.01	4.33 ± 0.09
4.01	9.68×10^{19}	1.04 ± 0.04	1.95 ± 0.08	40.00	9.66×10^{20}	1.00 ± 0.02	2.50 ± 0.09	500.00	8.86×10^{21}	0.28 ± 0.01	4.41 ± 0.09
4.91	1.19×10^{20}	1.05 ± 0.03	1.89 ± 0.07	60.00	1.45×10^{21}	1.00 ± 0.01	2.52 ± 0.10	602.00	9.80×10^{21}	0.24 ± 0.05	4.01 ± 0.11
7.51	1.81×10^{20}	0.96 ± 0.20	1.80 ± 0.34	80.00	1.93×10^{21}	0.91 ± 0.01	3.44 ± 0.10	702.00	1.06×10^{22}	0.19 ± 0.05	3.79 ± 0.10
10.03	2.42×10^{20}	0.96 ± 0.11	2.17 ± 0.20	100.00	2.40×10^{21}	0.90 ± 0.01	3.26 ± 0.11	862.50	1.16×10^{22}	0.18 ± 0.04	3.51 ± 0.08
13.49	3.26×10^{20}	0.86 ± 0.07	2.54 ± 0.17	154.00	3.62×10^{21}	0.71 ± 0.01	4.57 ± 0.10	862.50	1.16×10^{22}	0.16 ± 0.03	3.10 ± 0.07
14.96	3.61×10^{20}	0.92 ± 0.09	1.90 ± 0.24	218.50	4.93×10^{21}	0.55 ± 0.01	4.58 ± 0.09	908.50	1.18×10^{22}	0.15 ± 0.20	2.48 ± 0.34
19.99	4.83×10^{20}	0.87 ± 0.06	2.37 ± 0.10								

N_2 Data at 250 K

$p(N_2)^a$	$[N_2]^b$	$k_1{}^c$	$k_2{}^c$	$p(N_2)^a$	$[N_2]^b$	$k_1{}^c$	$k_2{}^c$	$p(N_2)^a$	$[N_2]^b$	$k_1{}^c$	$k_2{}^c$
3.98	1.11×10^{20}	1.28 ± 0.11	2.31 ± 0.20	30.00	8.46×10^{20}	1.49 ± 0.08	1.74 ± 0.11	200.50	5.49×10^{21}	0.74 ± 0.05	5.31 ± 0.05
5.98	1.67×10^{20}	1.45 ± 0.10	2.06 ± 0.18	40.00	1.14×10^{21}	1.39 ± 0.06	1.88 ± 0.10	305.50	7.54×10^{21}	0.68 ± 0.03	4.61 ± 0.04
7.98	2.24×10^{20}	1.46 ± 0.08	2.20 ± 0.13	50.00	1.43×10^{21}	1.33 ± 0.05	1.98 ± 0.03	408.00	9.02×10^{21}	0.50 ± 0.03	4.29 ± 0.04
9.98	2.79×10^{20}	1.33 ± 0.09	2.48 ± 0.17	58.00	1.65×10^{21}	1.31 ± 0.03	2.97 ± 0.05	600.50	1.09×10^{22}	0.38 ± 0.02	4.00 ± 0.03
12.00	3.36×10^{20}	1.31 ± 0.05	1.94 ± 0.15	78.00	2.24×10^{21}	1.16 ± 0.05	3.48 ± 0.08	696.50	1.16×10^{22}	0.30 ± 0.02	4.09 ± 0.03
14.99	4.19×10^{20}	1.29 ± 0.06	3.16 ± 0.20	98.50	2.85×10^{21}	0.96 ± 0.03	4.05 ± 0.05	795.00	1.22×10^{22}	0.30 ± 0.02	3.79 ± 0.03

Helium Data at 300 K

$p(He)^a$	$[He]^b$	$k_1{}^c$	$k_2{}^c$	$p(He)^a$	$[He]^b$	$k_1{}^c$	$k_2{}^c$	$p(He)^a$	$[He]^b$	$k_1{}^c$	$k_2{}^c$
2.01	4.85×10^{19}	1.00 ± 0.10	1.94 ± 0.19	8.22	1.99×10^{20}	0.94 ± 0.03	1.86 ± 0.06	104.50	2.41×10^{21}	0.94 ± 0.04	2.55 ± 0.09
3.00	7.24×10^{19}	0.98 ± 0.06	1.89 ± 0.12	12.00	2.90×10^{20}	0.98 ± 0.03	1.98 ± 0.06	149.00	3.37×10^{21}	0.90 ± 0.03	2.75 ± 0.08
4.00	9.66×10^{19}	0.91 ± 0.04	1.65 ± 0.08	15.00	3.62×10^{20}	0.96 ± 0.03	1.99 ± 0.05	203.00	4.49×10^{21}	1.03 ± 0.03	2.45 ± 0.08
5.00	1.21×10^{20}	0.93 ± 0.04	1.71 ± 0.08	20.00	4.83×10^{20}	0.91 ± 0.03	2.07 ± 0.05	304.00	6.45×10^{21}	0.72 ± 0.02	2.94 ± 0.08
5.00	1.21×10^{20}	0.95 ± 0.03	1.73 ± 0.07	30.00	7.24×10^{20}	0.93 ± 0.02	2.14 ± 0.04	406.00	8.27×10^{21}	0.70 ± 0.02	3.61 ± 0.10
6.00	1.45×10^{20}	0.93 ± 0.04	1.62 ± 0.07	52.00	1.26×10^{21}	0.98 ± 0.06	2.14 ± 0.13	502.00	9.87×10^{21}	0.56 ± 0.02	3.86 ± 0.13
7.00	1.69×10^{20}	0.96 ± 0.03	1.77 ± 0.07	81.50	1.97×10^{21}	1.00 ± 0.05	2.68 ± 0.11	601.50	1.14×10^{22}	0.60 ± 0.02	3.61 ± 0.14
7.98	1.93×10^{20}	0.94 ± 0.03	1.75 ± 0.06								

Argon Data at 300 K

$p(Ar)^a$	$[Ar]^b$	$k_1{}^c$	$k_2{}^c$	$p(Ar)^a$	$[Ar]^b$	$k_1{}^c$	$k_2{}^c$	$p(Ar)^a$	$[Ar]^b$	$k_1{}^c$	$k_2{}^c$
0.05	1.21×10^{18}	0.84 ± 0.39	1.48 ± 0.76	2.30	5.55×10^{19}	1.07 ± 0.08	1.95 ± 0.15	60.00	1.45×10^{21}	1.07 ± 0.19	5.11 ± 0.34
0.08	1.81×10^{18}	0.94 ± 0.28	1.56 ± 0.56	2.50	6.04×10^{19}	1.05 ± 0.09	2.12 ± 0.17	80.00	1.93×10^{21}	1.11 ± 0.13	4.95 ± 0.27
0.10	2.41×10^{18}	1.04 ± 0.17	1.79 ± 0.35	3.00	7.24×10^{19}	0.94 ± 0.07	2.47 ± 0.14	100.00	2.53×10^{21}	1.10 ± 0.10	4.62 ± 0.21
0.15	3.62×10^{18}	0.94 ± 0.10	1.85 ± 0.19	3.80	9.17×10^{19}	1.00 ± 0.05	2.02 ± 0.11	125.00	3.17×10^{21}	1.12 ± 0.13	5.12 ± 0.27
0.20	4.83×10^{18}	0.94 ± 0.07	1.65 ± 0.02	5.00	1.21×10^{20}	1.07 ± 0.04	2.13 ± 0.08	207.50	5.25×10^{21}	0.72 ± 0.05	5.08 ± 0.12
0.30	7.24×10^{18}	0.97 ± 0.05	1.72 ± 0.08	5.00	1.21×10^{20}	1.00 ± 0.10	2.02 ± 0.21	315.50	7.57×10^{21}	0.53 ± 0.02	4.93 ± 0.10
0.40	9.66×10^{18}	0.91 ± 0.03	1.70 ± 0.07	8.00	1.93×10^{20}	1.12 ± 0.08	2.25 ± 0.12	409.00	9.18×10^{21}	0.38 ± 0.01	4.73 ± 0.09
0.50	1.21×10^{19}	0.89 ± 0.03	1.78 ± 0.06	10.00	2.41×10^{20}	0.98 ± 0.04	2.01 ± 0.08	512.50	1.06×10^{22}	0.35 ± 0.01	4.85 ± 0.10
0.60	1.45×10^{19}	0.95 ± 0.03	1.85 ± 0.06	15.00	3.62×10^{20}	1.05 ± 0.03	2.51 ± 0.06	609.00	1.17×10^{22}	0.29 ± 0.10	4.08 ± 0.09
0.80	1.93×10^{19}	0.95 ± 0.02	1.77 ± 0.05	20.00	4.83×10^{20}	0.95 ± 0.03	2.28 ± 0.06	702.00	1.25×10^{22}	0.32 ± 0.01	3.84 ± 0.08
0.90	2.17×10^{19}	0.81 ± 0.02	1.45 ± 0.04	30.00	7.24×10^{20}	1.20 ± 0.02	2.22 ± 0.04	797.00	1.32×10^{22}	0.28 ± 0.01	3.71 ± 0.08
1.80	4.35×10^{19}	1.04 ± 0.09	2.11 ± 0.18	45.00	1.09×10^{21}	1.01 ± 0.02	2.64 ± 0.06				

Xenon Data at 300 K

$p(Xe)^a$	$[Xe]^b$	$k_1{}^c$	$k_2{}^c$	$p(Xe)^a$	$[Xe]^b$	$k_1{}^c$	$k_2{}^c$	$p(Xe)^a$	$[Xe]^b$	$k_1{}^c$	$k_2{}^c$
0.05	1.21×10^{18}	0.99 ± 0.29	1.56 ± 0.58	0.15	3.62×10^{18}	0.96 ± 0.07	1.83 ± 0.15	0.35	8.45×10^{18}	0.93 ± 0.03	1.50 ± 0.06
0.08	1.81×10^{18}	0.89 ± 0.16	1.54 ± 0.31	0.20	4.83×10^{18}	0.92 ± 0.05	1.66 ± 0.09	0.40	9.66×10^{18}	1.07 ± 0.04	1.62 ± 0.08
0.10	2.41×10^{18}	0.91 ± 0.10	1.72 ± 0.20	0.30	7.24×10^{18}	0.96 ± 0.04	1.64 ± 0.08				

SF_6 data at 300 K

$p(SF_6)^a$	$[SF_6]^b$	$k_1{}^c$	$k_2{}^c$	$p(SF_6)^a$	$[SF_6]^b$	$k_1{}^c$	$k_2{}^c$	$p(SF_6)^a$	$[SF_6]^b$	$k_1{}^c$	$k_2{}^c$
0.04	1.04×10^{18}	0.98 ± 0.07	2.04 ± 0.14	0.10	2.56×10^{18}	1.15 ± 0.17	2.26 ± 0.34	0.20	5.17×10^{18}	1.01 ± 0.11	2.12 ± 0.21
0.06	1.60×10^{18}	1.00 ± 0.11	1.96 ± 0.21	0.14	3.65×10^{18}	1.11 ± 0.10	2.07 ± 0.20	0.30	7.76×10^{18}	1.01 ± 0.07	1.98 ± 0.14
0.08	2.04×10^{18}	1.06 ± 0.10	2.07 ± 0.20								

CO_2 data at 300 K

$p(CO_2)^a$	$[CO_2]^b$	$k_1{}^c$	$k_2{}^c$	$p(CO_2)^a$	$[CO_2]^b$	$k_1{}^c$	$k_2{}^c$	$p(CO_2)^a$	$[CO_2]^b$	$k_1{}^c$	$k_2{}^c$
0.10	9.05×10^{17}	0.94 ± 0.12	1.74 ± 0.25	0.50	1.10×10^{19}	1.02 ± 0.07	2.01 ± 0.14	2.50	6.29×10^{19}	1.05 ± 0.08	1.96 ± 0.16
0.14	1.62×10^{18}	0.96 ± 0.13	1.85 ± 0.26	0.60	1.37×10^{19}	1.05 ± 0.06	2.03 ± 0.12	3.00	7.52×10^{19}	1.05 ± 0.07	1.98 ± 0.14
0.19	2.86×10^{18}	1.06 ± 0.10	1.94 ± 0.20	0.80	1.92×10^{19}	1.05 ± 0.04	1.88 ± 0.09	4.00	9.97×10^{19}	1.09 ± 0.06	2.10 ± 0.12
0.20	3.02×10^{18}	1.02 ± 0.21	1.84 ± 0.42	0.90	2.19×10^{19}	1.03 ± 0.04	1.95 ± 0.07	5.00	1.24×10^{20}	0.99 ± 0.05	2.04 ± 0.11
0.29	5.34×10^{18}	1.05 ± 0.07	1.95 ± 0.15	1.50	3.77×10^{19}	1.00 ± 0.11	1.85 ± 0.22	6.00	1.49×10^{20}	0.96 ± 0.05	2.17 ± 0.11
0.30	5.54×10^{18}	0.98 ± 0.13	1.96 ± 0.25	2.00	5.04×10^{19}	0.97 ± 0.09	1.96 ± 0.18	6.90	1.71×10^{20}	0.98 ± 0.04	1.99 ± 0.10
0.40	8.22×10^{18}	1.01 ± 0.08	1.86 ± 0.17								

[a] Partial pressure of the species, given in bar. [b] Concentration of the species, given in molecules cm^{-3}. [c] Rate constant, given in units of 10^{-11} cm^3 $molecule^{-1}$ s^{-1}.

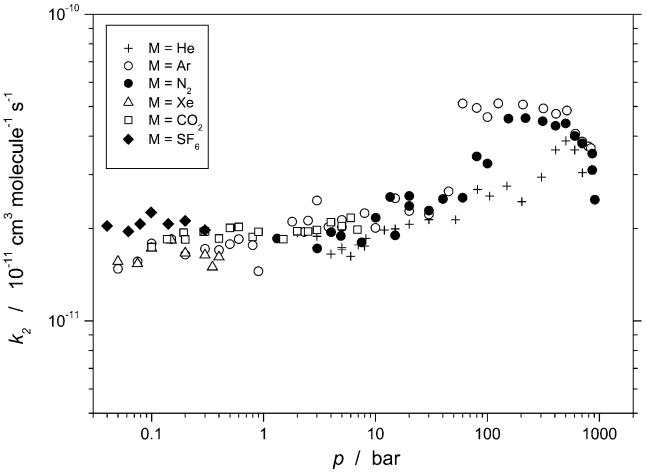

Figure 3. Combination rate constants of $CCl_3 + Br (+ M) \rightarrow CCl_3Br (+ M)$ (reaction 2) at 300 K; measurements in this work were made in the bath gases helium, argon, xenon, N_2, CO_2, and SF_6.

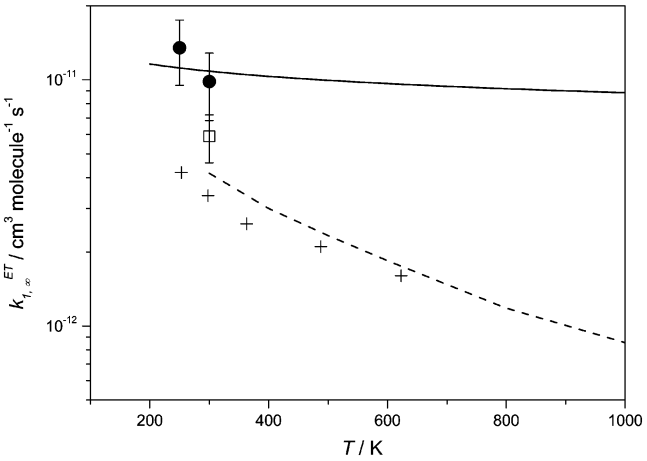

Figure 4. Temperature dependence of the limiting "high-pressure" rate constant, $k_{1,\infty}^{ET}(T)$. Experimental data were taken from (●) this work, (□) ref 14, and (+) ref 15; theoretical predictions were (—) from this work and (− − −) from ref 34.

bar, regardless of the bath gas, allowed us to directly determine the limiting "high-pressure" rate constant to be $k_{2,\infty}^{ET} = (2.0 \pm 0.2) \times 10^{-11}$ cm^3 molecule^{-1} s^{-1}. Compared to k_1, a more distinct increase of k_2 at pressures of >10 bar was observed in the bath gases N_2 and argon, and even in helium, a small increase of the rate constants was clearly observed at pressures of >100 bar. In N_2 and argon, the onset of diffusion control is again well seen, but it occurs at higher pressures than that observed in reaction 1.

The derived values for $k_{1,\infty}^{ET}$ and $k_{2,\infty}^{ET}$, such as those observed over more than 2 orders of magnitude in pressure and at two temperatures (250 and 300 K; compare, e.g., Figure 4), are summarized as

$$k_{1,\infty}^{ET}(T) = (1.0 \pm 0.2) \times 10^{-11}\left(\frac{T}{300\ \mathrm{K}}\right)^{-0.83} \mathrm{cm^3\,molecule^{-1}\,s^{-1}} \quad (6)$$

$$k_{2,\infty}^{ET}(T) = (2.0 \pm 0.2) \times 10^{-11}\left(\frac{T}{300\ \mathrm{K}}\right)^{-0.49} \mathrm{cm^3\,molecule^{-1}\,s^{-1}} \quad (7)$$

The given error limits in eqs 6 and 7 not only refer to the scatter of data but also include estimated systematic errors.

Pressure effects such as those illustrated in Figure 3 have rarely been reported before. They present the most important result of our work and call for a detailed analysis. We have strong evidence that these results are not due to the pressure dependence of the absorption at our observation wavelength. First propositions about the origin of the observed effects are given below. Because the characterization of the RC mechanism involves several elements of the ET mechanism, the latter also must be analyzed in detail. This will be done in the following section.

Discussion

A. Experimental "High-Pressure" Rate Constant, k_∞^{ET}. Reaction 1 has been studied previously[22−26] as a part of complex reaction mechanisms, which led to fitted values of k_1 between 1.7×10^{-13} and 1.2×10^{-11} cm^3 molecule^{-1} s^{-1}. A more direct access to k_1 was provided by Danis et al.[14] and by Ellermann,[15] whose results can be compared with our present data. Both groups monitored the recombination of CCl_3 radicals by transient UV spectroscopy. Their limiting "high-pressure" values are somewhat smaller than our results, which needs an explanation. Figure 4 compares the different data.

In their study, Danis et al.[14] generated CCl_3 radicals via the flash photolysis of Cl_2, which was followed by the reaction $Cl + CHCl_3 \rightarrow HCl + CCl_3$. On the basis of a Rice−Ramsperger−Kassel−Marcus (RRKM) modeling, the authors concluded that, under N_2 pressures of ∼1 bar, reaction 1 was near the high-pressure limit. With their assumption, they derived the relation $k_{1,\infty} = (3.3 \pm 0.8) \times 10^{-12}\,(T/298\ \mathrm{K})^{-1.0 \pm 0.2}$ cm^3 molecule^{-1} s^{-1}. This result is considerably lower than our $k_{1,\infty}$ value and also shows a much stronger temperature dependence.

A second direct measurement of reaction 1 was reported by Ellermann,[15] who generated CCl_3 radicals via the secondary reaction of $F + CHCl_3 \rightarrow HF + CCl_3$, following pulse radiolysis of SF_6. He reported a rate constant of $k_1 = (5.9 \pm 1.3) \times 10^{-12}$ cm^3 molecule^{-1} s^{-1} in 1 bar of SF_6 at 298 K. This value is a factor of ∼1.7 higher than the value from Danis et al.,[14] but it is still lower than our result. Our production of CCl_3 radicals via the laser photolysis of CCl_3Br probably presented the most direct approach such that the least complications are expected. There is the additional advantage that the absorption bands of the CCl_3 radical and the precursor overlap much less when CCl_3-Br instead of $CHCl_3$ is chosen. For this reason, we consider our results for $k_{1,\infty}^{ET}$ to be the most reliable.

The reasons for the differences between our results for $k_{1,\infty}^{ET}$ and those of Danis et al. in N_2[14] and Ellermann et al. in SF_6[15] cannot all be found; however, some appear rather clear. With efficient colliders, such as SF_6 used in ref 15, $k_{1,\infty}^{ET}$ is definitely reached in measurements at 1 bar. However, in 1 bar of N_2 at 300 K, such as the conditions used in ref 14, one approaches the high-pressure limit closely but not completely. On this basis, the apparent negative temperature dependence of ref 14 in part can be attributed to fall-off effects and most of the differences to our results can be understood. As the fall-off curves are shifted with temperature, the measurements of k_1 in 1 bar of N_2 fall further below $k_{1,\infty}^{ET}$ at higher temperatures.

A study on the combination reaction of CCl_3 radicals with bromine was reported by Fenter et al.,[25] using CCl_3Br as a precursor, similar to that done in the present work. Pressures in the range of 0.03−1 bar of the N_2 bath gas and temperatures of 298 and 333 K were used. Using a fall-off extrapolation with a center broadening factor $F_c = 0.6$, these authors determined the limiting low- and high-pressure rate constants as $k_{2,0}(300\ \mathrm{K}) = [N_2](5.2 \pm 3.0) \times 10^{-28}$ cm^6 molecule^{-2} s^{-1} and $k_{2,\infty}$-

(300 K) = (7.6 ± 0.6) × 10^{-11} cm^3 $molecule^{-1}$ s^{-1}. This value for $k_{2,\infty}$ is more than 3 times higher than our value. The parameter $k_{2,\infty}$ was optimized using the kinetic model based on reactions 1−5. In contrast to the results from the present work, however, reaction 1 was assumed to be given by the small value $k_{1,\infty}$(300 K) = (3.3 ± 0.8) × 10^{-12} cm^3 $molecule^{-1}$ s^{-1} from ref 14 and, thus, was assumed to be insignificant. In this case, the CCl_3 radicals would be removed predominantly via reaction 2, which results in the larger values of k_2. Using the present value of $k_{1,\infty}$, a reinterpretation of the experiments of ref 25 would have led to near agreement with the present results.

B. Theoretical Analysis of the Derived "High-Pressure" Rate Constant, k_∞^{ET}. To rationalize contributions from a RC mechanism to k_1 and k_2, see below, it seems necessary to analyze the experimental "high-pressure" rate constants $k_{1,\infty}^{ET}$ and $k_{2,\infty}^{ET}$. This can be done on the basis of statistical adiabatic channel/classical trajectory (SACM/CT) calculations such as those described in the work of Maergoiz et al.[27,28] In this treatment, k_∞^{ET} is represented by an upper limit given by phase space theory (PST) and a rigidity factor (f_{rigid}) that results from the anisotropy of the potential. It should be mentioned that k_∞^{ET} is reported here as the capture rate constant multiplied by an electronic weight factor α_{spin} ($^1/_4$ for reaction 1 and of $^1/_8$ for reaction 2; see below). The parameter $k_\infty^{ET,PST}$ is determined by the interaction potential between the radicals, neglecting the anisotropy. First, we investigated whether this potential for reaction 1 can be represented by a dipole−dipole potential. A calculation of the dipole moment of CCl_3 radicals on the UB3LYP level with 6-31G (d,p) basis set[29] led to a value of 0.22 D. However, more-appropriate RCCSD(T) calculations[30] with an aug-cc-pVTZ basis set on a CEPA-1 geometry[31] led to a smaller value, 0.091 D. This value indicates that the long-range dipole−dipole potential is irrelevant for the present conditions. Instead, we characterized the interaction between two CCl_3 radicals by a Morse potential;[27,28] the parameters r_e = 2.61 Å, β = 1.88 $Å^{-1}$, and D_0 = 2.46 × 10^4 cm^{-1} were estimated for reaction 1, whereas for reaction 2, we used r_e = 2.48 Å, β = 0.94 $Å^{-1}$, and D_0 = 1.96 × 10^4 cm^{-1}. This leads to[27,28] $k_{1,\infty}^{ET,PST}$ = 6.0 × 10^{-11} cm^3 $molecule^{-1}$ s^{-1} and $k_{2,\infty}^{ET,PST}$ = 1.5 × 10^{-10} cm^3 $molecule^{-1}$ s^{-1} at 300 K. In comparison to the experimental results, experimental rigidity factors of $f_{rigid,1}^{expt}$ ≈ 0.17 and $f_{rigid,2}^{expt}$ ≈ 0.14 arise. Note that the dipole−dipole potential would have led to f_{rigid} = 0.385.[32] For a purely theoretical estimate of f_{rigid}, we use standard valence potentials such as those proposed by Cobos and Troe[33] (i.e., parameters $\alpha/\beta \approx 0.5$) and evaluated by SACM/CT in refs 27 and 28. Calculating the anisotropy parameters $C = (\epsilon_e^2/2B_\infty D_0)$ with estimated values ϵ_e = 167 cm^{-1}, B_∞ = 0.15 cm^{-1}, and D_0 = 2.46 × 10^4 cm^{-1} for reaction 1 (and ϵ_e = 187 cm^{-1}, B_∞ = 0.17 cm^{-1}, and D_0 = 1.96 × 10^4 cm^{-1} for reaction 2) (here, B_∞ is the total rotational constants of the CCl_3 radical, including its relative motion with the reaction partner) leads to C_1 = 3.74 and C_2 = 5.33, and from this,[27,28] $f_{rigid,1} \approx 0.16$ and $f_{rigid,2} \approx 0.08$. These values are not too far from the experimental f_{rigid}^{expt} value (currently, only estimates of the described type are possible, as long as ab initio potentials are not available). A consequence of the assumption of a standard valence potential with $\alpha/\beta \approx 0.5$ is the prediction[27,28] of almost-temperature-independent k_∞^{ET} such as that observed also in our work. This is in contrast to the marked negative temperature dependence suggested by canonical variational transition-state theory in the treatment from Pesa et al.[34] (see Figure 4). However, there are known problems with canonical transition-state theory, in addition to the uncertainty of the potential such that the present prediction seems more probable.

It will be shown below that the analysis of k_∞^{ET}, in terms of $k_\infty^{ET,PST}$ and the rigidity factor f_{rigid}, is of major importance for an analysis of recombination rate constants in the RC mechanism. This explains why we have given a detailed interpretation of the measured $k_{1,\infty}^{ET}$ and $k_{2,\infty}^{ET}$ values.

C. Transition to Diffusion-Controlled Kinetics. To identify possible contributions from the RC mechanism at the low-pressure side, the values of k_∞^{ET} have been determined. At the high-pressure side, the values of the recombination rate constants under diffusion-controlled conditions need to be specified, which then allows the additional contributions such as those appearing in Figures 2 and 3 to be identified. The combination rate constants in the gas-to-liquid transition range traditionally have been approximated by the relationship

$$k_{observed} = \frac{k_{rec} k_{diff}}{k_{rec} + k_{diff}} \tag{8}$$

(See, e.g., ref 19.) In eq 8, k_{rec} is the hypothetical value of the combination rate constants in the absence of diffusion control (i.e., in the present case, the joint contribution from the ET mechanism and the RC mechanism (see below)) and k_{diff} is the value of the rate constant for assumed complete diffusion control for the combination process. Toward low densities, diffusion becomes faster; k_{diff} increases sharply and governs the denominator in eq 8, which leads to

$$k_{observed} \rightarrow k_{rec} \tag{9}$$

For high densities, diffusion slows and finally controls the combination reaction.

$$k_{observed} \rightarrow k_{diff} \tag{10}$$

The rate constant at diffusion control (k_{diff}) is given by

$$k_{diff} = 4\pi\alpha_{spin}(M)RD \tag{11}$$

where D is the diffusion coefficient of the recombining radicals in the bath medium and R is the effective capture distance. The (density-dependent) electronic weight factor $\alpha_{spin}(M)$ must be included, as is done for k_{rec}. In solution kinetics, the limiting spin-statistical value of α_{spin} (e.g., $^1/_4$ or $^1/_8$ in reactions 1 or 2, respectively) is often simply assumed without convincing evidence. However, this is only valid as long as spin-changing transition rates are much slower than diffusion rates that separate non-spin-matching radical reactants, even under the influence of very frequent collisions of the bath gas and the minor energy differences (ΔE) involved. Obviously, the continuous decrease of k_{diff} with density always must lead to a relaxation of this condition and a transition of $\alpha_{spin}(M) \rightarrow 1$. Unfortunately, there are no real quantitative calculations currently available, predicting where to expect this in a given system. For some further discussion, see Section E of the Discussion.

The correct choice of R has been the subject of controversial discussions. On the basis of the analysis of Section B of the Discussion, it seems most reasonable to identify R with the thermally averaged capture cross section $\langle\sigma\rangle$ of CCl_3 radicals at the limiting "high-pressure" rate constant:[28]

$$R = \sqrt{\frac{\langle\sigma\rangle}{\pi}} = \left[\left(\frac{1}{\pi f}\right)\left(\frac{k_\infty^{ET}}{\alpha_{spin}(M)}\right)\sqrt{\frac{\pi\mu}{8kT}}\right]^{1/2} \tag{12}$$

where $f = {}^1/_2$ for identical reactants and $f = 1$ for different reactants; μ is the reduced mass of two radicals. From this, values of $R = 2.8$ Å for reaction 1 and $R = 3.8$ Å for reaction 2 were derived. To reconvert k_∞^{ET} to the "unrestricted" capture rate constant at this stage, we must use an α_{spin} value of ${}^1/_4$ for reaction 1 and ${}^1/_8$ for reaction 2, as previously mentioned.

Tracer diffusion coefficients of radicals in the medium-density region of supercritical fluids are mostly unknown. Diffusion coefficients in the medium-density range cannot be well-extrapolated[35] from low-pressure gas phase using the Chapman−Enskog kinetic theory[36] or from the liquid phase using the Stokes−Einstein relationship;[37] both methods overestimate D. Instead, we used the successful semiempirical method to estimate the diffusion coefficient of an infinitely diluted solute in a solvent, as suggested in the work of Ruckenstein and Liu.[38,39] In these calculations,[39] the density-dependent diffusion coefficient can be estimated on the basis of the rough hard-sphere theory,[40−43] treating the intermolecular interaction between solute and solvent as a Lennard-Jones (LJ)-type fluid. The basic equation[39] can be written for the tracer diffusion coefficient of a solute in a real fluid following the LJ expression

$$D_{AM} = A_D D_{AM}^{LJ}(\rho^*, T^*; \sigma_{AM}^{eff}, \epsilon_{AM}^{eff})\chi \qquad (13)$$

where A_D is the rotational−translation coupling factor which attributes a reduction in diffusion to the nonsphericity of the molecules. The equation for a LJ fluid is related to that for a common hard-sphere fluid, but with the introduction of the attractive contribution and the effective hard-sphere diameter,[44] such as that shown in eq 40 of ref 39. The parameters ρ^* and T^* are the reduced density ($\rho^* = [M](\sigma_M^{eff})^3$) and the reduced temperature ($T^* = kT/\epsilon_M^{eff}$).

The aforementioned method is not intended for radicals; therefore, further improvement of the calculation would be necessary to exactly reproduce our experimental data quantitatively. For example, in the calculation of diffusion coefficients (such as that in eq 12), besides rotational−translation coupling, all other effects are neglected, such as anisotropic interactions, the increased dielectric friction in the higher-density region (because of the enhanced attractive intermolecular interaction between radicals and solvent molecules[45]), as well as the effect of overcoming the spin-limited reaction probability of radical pairs[46] in the excited electronic states at higher densities. Presently, we cannot provide a detailed theoretical analysis of these effects for the remaining differences (up to 1 order of magnitude) between the calculated values of k_1 and experimental data at the highest pressures (at >100 bar). Because the difference between calculated and observed values of k_1 in the diffusion limit concerns the absolute value but not the shape of the density dependence, we use a simple scaling approach as a sufficient approximation for our purpose, with an almost-constant scaling factor χ to correct for the neglected effects in k_{diff}. For simplicity, we only mention the values of the combination $\chi' = \alpha_{spin}\chi$ when D (from eq 13) is used in eq 11, because we currently cannot decide separately on the actual value of α_{spin} in the diffusion-limited density regime of our systems (see previous comments and Section E in the Discussion). To match the calculated k_{diff} values with the asymptotic experimental data, one finds $\chi_1' \approx 0.08$ for reaction 1 and $\chi_2' \approx 0.24$ for reaction 2. The relative ratio of χ_1/χ_2 (or, similarly, χ_1'/χ_2') should characterize the extent of favorable geometric structures of CCl_3...M complexes that occur in both reactions: CCl_3 radicals are more anisotropic, which affects the diffusion kinetics more than the isotropic Br atoms do, such that a smaller value for χ_1 seems reasonable. Figure 5 compares the results of the calculation of the diffusion rate constant and the diffusion limited k_1 with our experimental data in an argon bath gas near 300 K (here, without considering the contribution of the RC mechanism; see below). The diffusion rate constant at higher pressures is clearly limiting the kinetics at the highest pressures. The shaded area in Figure 5 reflects the uncertainty within the calculation.[39]

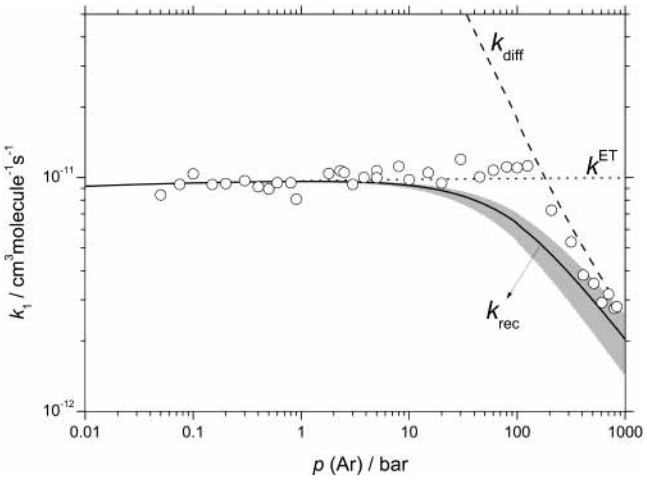

Figure 5. Combination rate constant k_1 in the argon bath gas at 300 K, showing the transition to the onset of diffusion control. Legend is as follows: (− − −) limiting diffusion-controlled rate constants, (· · ·) k^{ET} from the energy-transfer mechanism, and (—) rate constants without contribution from the radical−complex (RC) mechanism. Shaded area illustrates the error estimation of the calculation.[39]

D. Rate Constants at Elevated Pressures before the Onset of Diffusion Control. Figure 5 clearly shows that our experimental data for k_1 at pressures of 40−300 bar differ from an assumed smooth transition between energy-transfer- and diffusion-controlled kinetics. Such deviations are even more pronounced for the rate constants k_2 in the same pressure range, such as those observed in Figure 3. Because both rate constants were at the high-pressure limit of the conventional ET mechanism, the additional increase of the rate constants must be explained by other dynamic features, such as the RC mechanism of combination reactions or some density-dependent influence of excited electronic states. In the following, we first consider the RC mechanism.

For reaction 1, we choose the simple formulation for ET and RC mechanisms from reactions I and II, respectively (also see the examples in the reports from Troe and co-workers[4,9,10,47]). We assume that k_c and k_{-c} are always fast enough to maintain an equilibrium concentration of $[AM]_{eq}$, with

$$K_{eq} = \frac{[AM]_{eq}}{[A]_{eq}[M]} = \frac{[AM]_{eq}}{([A] - [AM]_{eq})[M]} \qquad (14a)$$

$$[AM]_{eq} = \frac{K_{eq}[A][M]}{1 + K_{eq}[M]} \qquad (14b)$$

where

$$[A]_{eq} = \frac{[A]}{1 + K_{eq}[M]}$$

Here, [A] denotes the total concentration, i.e., $[A]_{eq} + [AM]_{eq}$. K_{eq} is evaluated by the Bunker−Davidson expression,[48] which was shown to require some modifications.[49,50] In the expression of ref 48, dimers that are in metastable states (i.e., at energies

higher than the binding energy but below the centrifugal barrier) are not considered.[50] Schwarzer and Teubner derived a modified expression[50] for K_{eq} by decomposing the gas-phase radial distribution function into contributions that result from bound states and from scattering collisions (see Appendix B of ref 49). The calculated equilibrium constants are mostly in the range of $10^{-22}-10^{-23}$ cm^3 under our conditions.

The total rate constant from both mechanisms is then given by

$$k_{1,\mathrm{rec}} = k_1^{\mathrm{ET}} + k_1^{\mathrm{RC}} = \frac{k_{1,\infty}^{\mathrm{ET}} k_{1,0}{}^{\mathrm{ET}}[\mathrm{M}]}{k_{1,\infty}^{\mathrm{ET}} + k_{1,0}^{\mathrm{ET}}[\mathrm{M}]} F_{\mathrm{center}} + \frac{K_{\mathrm{eq}} k_{\mathrm{d}}[\mathrm{M}] + K_{\mathrm{eq}}^2 k_{\mathrm{e}}[\mathrm{M}]^2}{(1 + K_{\mathrm{eq}}[\mathrm{M}])^2} \quad (15)$$

k^{RC} has the limiting low- and high-pressure values:

$$k_0^{\mathrm{RC}} = K_{\mathrm{eq}} k_{\mathrm{d}}[\mathrm{M}] \qquad (\text{for } [\mathrm{M}] \rightarrow 0) \qquad (16a)$$

$$k_\infty^{\mathrm{RC}} = k_{\mathrm{e}} \qquad (\text{for } [\mathrm{M}] \rightarrow \infty) \qquad (16b)$$

For reaction 2, the analogous mechanisms that involve two nonidentical radicals must be considered and with

$$\mathrm{A} + \mathrm{M} \rightleftarrows \mathrm{AM} \qquad (K_{\mathrm{eq,A}}) \qquad (17a)$$

$$\mathrm{B} + \mathrm{M} \rightleftarrows \mathrm{BM} \qquad (K_{\mathrm{eq,B}}) \qquad (17b)$$

$$\mathrm{AM} + \mathrm{B} \rightarrow \mathrm{AB} + \mathrm{M} \qquad (k_{\mathrm{C}}) \qquad (17c)$$

$$\mathrm{A} + \mathrm{BM} \rightarrow \mathrm{AB} + \mathrm{M} \qquad (k_{\mathrm{D}}) \qquad (17d)$$

$$\mathrm{AM} + \mathrm{BM} \rightarrow \mathrm{AB} + 2\mathrm{M} \qquad (k_{\mathrm{E}}) \qquad (17e)$$

the overall combination rate constants are expressed as

$$k_{2,\mathrm{rec}} = \frac{k_{2,\infty}{}^{\mathrm{ET}} k_{2,0}{}^{\mathrm{ET}}[\mathrm{M}]}{k_{2,\infty}{}^{\mathrm{ET}} + k_{2,0}{}^{\mathrm{ET}}[\mathrm{M}]} F_{\mathrm{center}} + \frac{(K_{\mathrm{eq,A}} k_{\mathrm{C}} + K_{\mathrm{eq,B}} k_{\mathrm{D}})[\mathrm{M}] + K_{\mathrm{eq,A}} K_{\mathrm{eq,B}} k_{\mathrm{E}}[\mathrm{M}]^2}{(1 + K_{\mathrm{eq,A}}[\mathrm{M}])(1 + K_{\mathrm{eq,B}}[\mathrm{M}])} \quad (18)$$

At the densities considered, the concentration of the weakly bound bath-gas−radical complexes is at its equilibrium value at any time. From the equilibrium constant, the degree of complexation ([AM]/([AM] + [A]) is calculated as a function of bath gas, M, and temperature (see Figures 6a and b). The pronounced growth of the concentrations of complexed radicals at higher densities and lower temperatures is evident. Kinetic contributions of AM_n can also be similarly evaluated. However, under the experimental conditions, the relatively low concentrations and overlapping contributions of all possible combination channels will not result in pronounced individually identifiable contributions of the various sizes of AM_n. We thus assume that contributions of all complexes can formally be represented by expression 18 within our experimental limits.

Although AM concentrations influence (linearly or quadratically) k^{RC}, the competing ET dynamics is not restricted to the remaining and decreasing concentration of uncomplexed $[\mathrm{A}]_{\mathrm{eq}} = [\mathrm{A}] - [\mathrm{AM}]_{\mathrm{eq}}$. Radical complexes can also participate in an ET-type dynamics, e.g. AM + A + M → A_2M + M (or A_2 + 2M). Interesting differences may influence the shape of the pressure-dependent transition from k_0^{RC} to k_∞^{RC} in eq 16. If the AM radical complexes are very weak, with correspondingly short lifetimes of AM, the reactions really follow reaction II, according to the original "chaperon" model. In these cases, the reaction always occurs under dynamical "high-pressure conditions", i.e., "stabilization" of A_2 (by $A_2M \rightarrow A_2 + M$ or $A_2M_2 \rightarrow A_2 + 2M$) is faster than the alternative "redissociation" ($A_2M \rightarrow A + AM$ or $A_2M_2 \rightarrow AM + AM$). In all such cases, the transition of eq 16 corresponds to the same curve of transition $k_0 \rightarrow k_\infty$, which is simply the density-dependent increase and saturation of the AM concentration (neglecting here higher complexes). If, however, AM complexes are bound sufficiently strongly, fast stabilization of the A_2 or A_2M product from AM + AM by dissociation of an M is no longer automatically guaranteed. In such cases, even at the saturation level of AM concentration, the combination reaction may show further pressure dependence of the ET type, when the AM "complexes" then mainly behave like somewhat-larger ordinary molecules (AM + AM + M), stabilized by additional bath gas collisions.

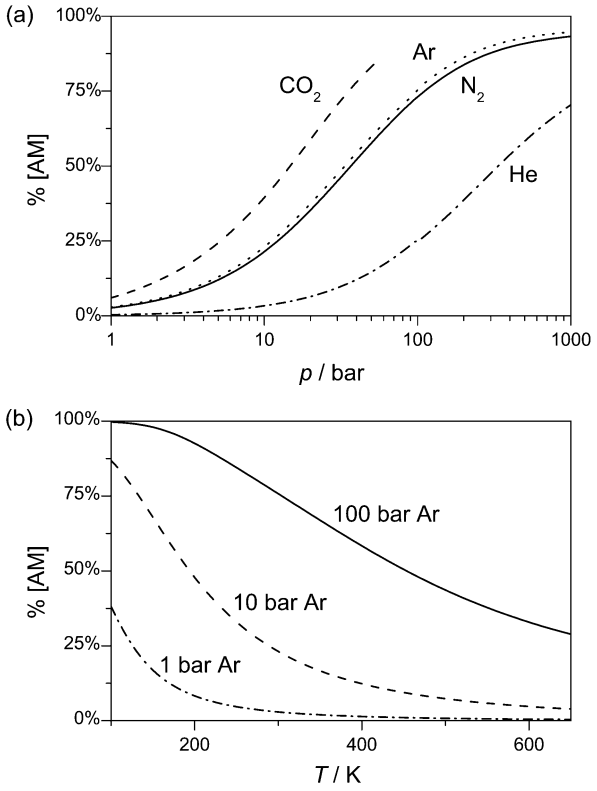

Figure 6. Degree of complexation for (a) the bath-gas dependence at 300 K for CCl_3 radicals and (b) the temperature dependence for CCl_3 radicals in argon at 100, 10, and 1 bar from the top.

Figure 7 shows a fit to the experimental data for reaction 1 in the argon bath gas at 300 K. The solid line considers the contribution from the usual ET mechanism and a possible contribution from the RC mechanism. As compared with the fit in Figure 5, the additional contribution from the RC mechanism results in a much better representation of the experimental data in the medium-density region. The same optimization was applied to the N_2 and helium data, and the fitting parameters derived are summarized in Table 2. The corresponding analysis of the CCl_3 + Br data (i.e., reaction 2) is illustrated for M = Ar in Figure 8, for M = N_2 in Figure 9, and for M = He in Figure 10. Again, in all three cases in which the increase of k_2 at higher densities was very pronounced, the experimental data were fully reproduced with the proposed mechanism and a minimum of fitting parameters, such as those summarized in Table 3. This consistent explanation of the observed unusual pressure dependences, in terms of a contribution from the RC mechanism, is the central result of this paper.

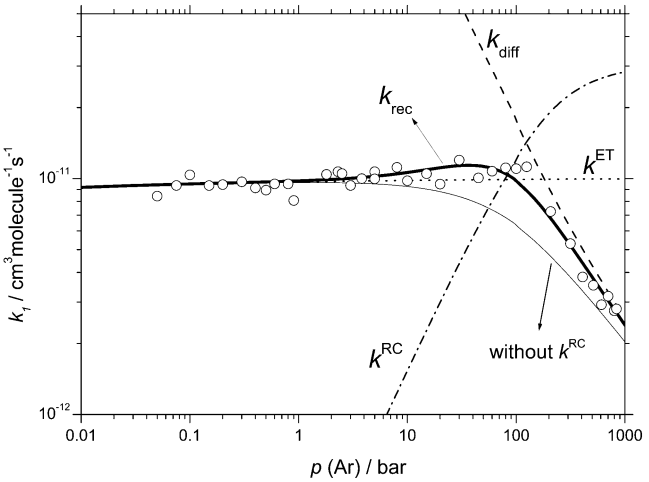

Figure 7. Combination rate constant k_1 in the argon bath gas at 300 K, showing the transition to the onset of diffusion control. Legend is as follows: (• • •) k^{ET} from the energy-transfer mechanism, (− − −) limiting diffusion-controlled rate constants, (− • −) and k^{RC} from the radical−complex mechanism. The thin solid line represents the resulting rate constants without k^{RC}, and the thick solid line represents the resulting rate constants including k^{RC}. Fitting parameters used in this calculation are summarized in Table 2.

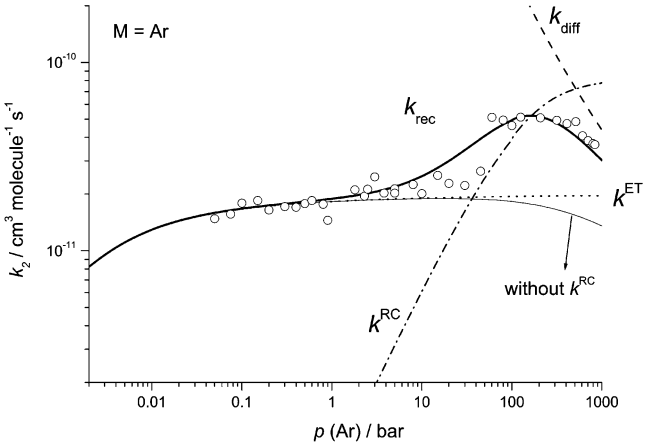

Figure 8. Same as Figure 7, for CCl_3 + Br at 300 K in argon.

TABLE 2: Kinetic Parameters for the CCl_3 + CCl_3 (+ M) → C_2Cl_6 (+ M) Reaction at 300 K

	ET	k_{diff}	RC			
M	k_∞^{ET} (cm^3 s^{-1})	χ_1'	k_{AM+A} (cm^3 s^{-1})	k_{AM+AM} (cm^3 s^{-1})	$k_{0,RC}$ (cm^6 s^{-1})	K_{eq}(AM) (cm^3)
Ar	1.0×10^{-11}	0.09	2.3×10^{-11}	3.8×10^{-11}	6.5×10^{-33}	2.9×10^{-22}
N_2	1.0×10^{-11}	0.08	1.8×10^{-11}	3.1×10^{-11}	4.9×10^{-33}	2.7×10^{-22}
He	1.0×10^{-11}	0.08	1.4×10^{-11}	2.2×10^{-11}	4.3×10^{-34}	3.0×10^{-23}

We have also observed this effect in an even more pronounced way for the larger benzyl radicals.[3]

The interpretation of our observations, in terms of a contribution from the RC mechanism, can only be correct if the rate constants for the reaction AM + AM are larger than the corresponding values for A + A (similarly, the reaction AM + BM should be faster than A + B). This hypothesis needs an explanation. The experimental fit, for example, suggested that k_{AM+AM} for A = CCl_3 and M = Ar was ∼3.8 times larger (and k_{AM+A} ∼2.3 times larger) than k_{A+A} ($k_{A+A} = k_{1,\infty}^{ET}$). Simple phase space theory does not predict such differences between k_{AM+AM}, k_{AM+A}, and k_{A+A}, because the effects of the different cross sections and reduced masses partially compensate. Thus, the differences between k_{AM+AM}, k_{AM+A}, and k_{A+A} can only be found in different rigidity factors (f_{rigid}). One may imagine that the presence of a van der Waals complex partner M shields and reduces the anisotropy of the valence potential between A and A. In the extreme, the value of f_{rigid} may approach unity. Having calculated K_{eq} in the described way, the fit of our experimental results in Figures 7 and 8 leads to the rate constants k_d and k_e, or k_C, k_D, and k_E. Using the calculated values of $k_{1,\infty}^{ET,PST}$ and $k_{2,\infty}^{ET,PST}$ from Section B in the Discussion, this leads to experimental f_{rigid} values for k_d and k_e (or k_C, k_D, and k_E) that differ in the different bath gases. For instance, f_{rigid}^{expt} for reaction 1 and k_{AM+AM} increases in the order He (∼0.38) < N_2 (∼0.54) < Ar (∼0.65). The observed value, e.g., for argon, is a factor of ∼4 larger than that for k_{A+A} (0.17) and still is below unity. Therefore, this interpretation seems to provide an internally consistent picture. Note that the f_{rigid}^{expt} values in k_{AM+A}, which increase in the order He (∼0.25) < N_2 (∼0.31) < Ar (∼0.39), lie between the f_{rigid}^{expt} values in k_{A+A} and k_{AM+AM}, which again is consistent with our postulate of a shielding effect. Presently, we cannot say whether this explanation is correct. Ab initio calculations of the AM + AM potential and CT calculations of capture on such potentials would be required to arrive at definite conclusions. Currently, we do not have such calculations. The apparent increase of the f_{rigid}^{expt} factors for k_{AM+BM} in CCl_3 + Br, rising from He (∼0.46) < N_2 (∼0.60) < Ar (∼0.66), leaves the value of $f_{rigid,2}^{expt}$ below unity. The rigidity factors, rising from He (∼0.27) < N_2 (∼0.30) < Ar (∼0.39) for k_{AM+B} and He (∼0.30) < N_2 (∼0.42) < Ar (∼0.39) for k_{A+BM} are also consistent with this interpretation.

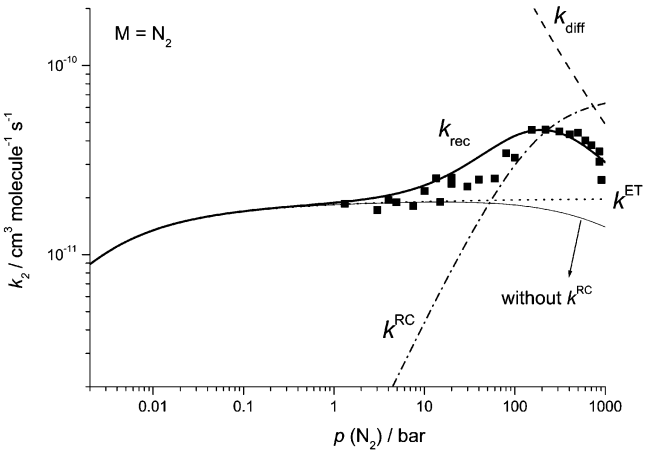

Figure 9. Same as Figure 7, for CCl_3 + Br at 300 K in N_2.

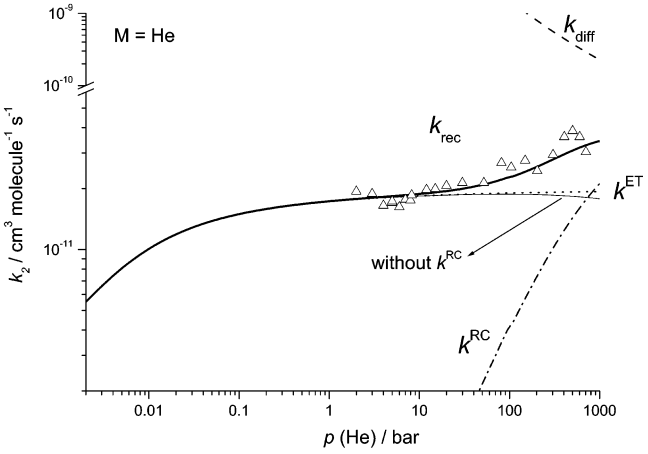

Figure 10. Same as Figure 7, for CCl_3 + Br at 300 K in helium.

TABLE 3: Kinetic Parameters for the $CCl_3 + Br (+ M) \rightarrow CCl_3Br (+ M)$ Reaction at 300 K

	ET	k_{diff}	RC (A = CCl_3, B = Br)					
M	k_∞^{ET} ($cm^3\ s^{-1}$)	χ_2'	k_{AM+B} ($cm^3\ s^{-1}$)	k_{BM+A} ($cm^3\ s^{-1}$)	k_{AM+BM} ($cm^3\ s^{-1}$)	$k_{0,RC}$ ($cm^6\ s^{-1}$)	K_{eq}(AM) (cm^3)	K_{eq}(BM) (cm^3)
Ar	2.0×10^{-11}	0.28	5.8×10^{-11}	6.2×10^{-11}	9.8×10^{-11}	2.7×10^{-32}	2.9×10^{-22}	1.7×10^{-22}
N_2	2.0×10^{-11}	0.24	4.5×10^{-11}	4.4×10^{-11}	8.8×10^{-11}	1.9×10^{-32}	2.7×10^{-22}	1.6×10^{-22}
He	2.0×10^{-11}	0.24	3.9×10^{-11}	3.9×10^{-11}	6.8×10^{-11}	1.9×10^{-33}	3.0×10^{-23}	1.7×10^{-23}

E. Density-Dependent Electronic Quenching, $\alpha_{spin}(M)$. The approach of two CCl_3 radicals in their doublet electronic ground states may lead to the electronic ground-state singlet C_2Cl_6 or to the excited triplet C_2Cl_6. The pure spin statistics ($\alpha_{spin}(M)$) tells us that only one-fourth of the $CCl_3 + CCl_3$ encounters succeed to form ground-state C_2Cl_6, whereas three-fourths of the encounters are unsuccessful because they separate before they can attain the "correct" spin configuration. Such a situation is most probable in low-pressure environments and not-too-high densities. Similarly, $\alpha_{spin}(M)$ studies indicate that one-eighth of the $CCl_3 + Br$ encounters have been included.[51,52] For an enhancement of the recombination probability at high densities (i.e., an increase of $\alpha_{spin}(M) \rightarrow 1$), at least two reasons must be considered. The underlying condition is that the rate constant of the electronic transition (here, triplet to singlet), k_{ISC}, of the reagents approaching each other not in the singlet ground state must become fast, compared to relevant translational motion, e.g., the diffusion process. With the asymptotically isoenergetic electronic states of our systems at very large distances, there is a range of moderate separations of the radicals where the energetic splitting between ground and excited states is really small and favorable for transitions. In many cases, collisions, especially with heavier atoms, increase spin−orbit coupling in the combined system (known as "external heavy atom effect") and thus accelerate electronic quenching. The number of bath-gas collisions, even within the time interval of very small diffusional displacements, becomes very high at high densities, which leads to the increasing probability to enter the ground-state surface in connection with multiple encounters. Increased spin−orbit coupling should also be considered, with respect to eventual "internal heavy atom effects" in RC units AM_n.

Even without collision-induced electronic quenching, however, the increase of density alone must lead to a breakdown of the condition of a "spin-statistic" α_{spin} ($^1/_4$ or $^1/_8$). The strong decrease of the diffusion rate with density alone is sufficient to arrive at a point where it is not bigger than k_{ISC}. Unfortunately, a quantitative understanding of this important problem in atom and radical combinations is still lacking,[53,54] and thus usable predictions or calculations for which to compare are not available. From our experimental evidence, we currently cannot confirm the simple, extreme assumption that all changes in $\alpha_{spin}(M)$ in our systems occur only at much higher densities than applied here. Contributions of changing $\alpha_{spin}(M)$ to our observation cannot be ruled out; however, there is also no direct experimental evidence for them. Further experimental studies are planned to clarify the situation on the basis of, for example, heavy-mass bath-gas influences in selected systems.

Conclusions

The combination reactions $CCl_3 + CCl_3 (+ M) \rightarrow C_2Cl_6 (+ M)$ and $CCl_3 + Br (+ M) \rightarrow CCl_3Br (+ M)$ (with rate constants of k_1 and k_2, respectively) were studied at 250 and 300 K over the pressure range of 0.01−1000 bar in the bath gases helium, argon, xenon, N_2, CO_2, and SF_6. The rate constants of reactions 1 and 2 reached a pressure-independent range at ∼1−10 bar, such that the limiting "high-pressure" rate constants of the energy-transfer (ET) mechanism $k_{1,\infty}^{ET}$ and $k_{2,\infty}^{ET}$ could be determined over a sufficiently wide pressure range. Our results can be represented by

$$k_{1,\infty}^{ET} = (1.0 \pm 0.2) \times 10^{-11}(T/300\ K)^{-0.17}$$
$$(cm^3\ molecule^{-1}\ s^{-1})$$

and

$$k_{2,\infty}^{ET} = (2.0 \pm 0.2) \times 10^{-11}(T/300\ K)^{-0.13}$$
$$(cm^3\ molecule^{-1}\ s^{-1})$$

These values were analyzed in terms of statistical adiabatic channel/classical trajectory (SACM/CT) theory. An interpretation of the observed increase in the rate constants between ∼40 bar and the onset of diffusion-limited dynamics was given in terms of a radical−complex mechanism. Our analysis provides a consistent description. However, more-quantitative conclusions must wait until more theoretical information on the potentials and dynamics of the radical complexes involved is available. A better understanding of the collision-induced electronic quenching is also required.

Acknowledgment. Financial support of this work by the Deutsche Forschungsgemeinschaft (Sonderforschungsbereich 357 "Molekulare Mechanismen Unimolekularer Prozesse"), as well as helpful discussions with T. Lenzer, V. Ushakov, A. Maergoiz, M. Teubner, D. Schwarzer, J. Schroeder, and P. Botschwina, are gratefully acknowledged. K. O. is deeply indebted to V. Ushakov for generous and invaluable discussions during this work. K. O. also thanks the Alexander von Humboldt Foundation for the funding of her work within the "Sofja Kovalevskaja Program".

References and Notes

(1) Rabinowitch, E. *Trans. Faraday Soc.* **1937**, *33*, 283.
(2) Porter, G.; Smith, J. A. *Proc. R. Soc. London A* **1961**, *261*, 28.
(3) Oum, K. W.; Sekiguchi, K.; Luther, K.; Troe, J. *Phys. Chem. Chem. Phys.* **2003**, *5*, 2931.
(4) Hippler, H.; Rahn, R.; Troe, J. *J. Chem. Phys.* **1990**, *93*, 6560.
(5) Gao, D. F.; Stockwell, W. R.; Milford, J. B. *J. Geophys. Res., [Atmos.]* **1995**, *100*, 23153.
(6) Hansen, J. C.; Francisco, J. S. *Chem. Phys. Chem.* **2002**, *3*, 833.
(7) Hippler, H.; Luther, K.; Troe, J. *Chem. Phys. Lett.* **1972**, *16*, 174.
(8) Hippler, H.; Luther, K.; Troe, J. *Ber. Bunsen Phys. Chem.* **1973**, *77*, 1020.
(9) Hippler, H.; Troe, J. *Int. J. Chem. Kinet.* **1976**, *8*, 501.
(10) Baer, S.; Hippler, H.; Rahn, R.; Siefke, M.; Seitzinger, N.; Troe, J. *J. Chem. Phys.* **1991**, *95*, 6463.
(11) Stark, H. Ph.D. Thesis, Göttingen University, Göttingen, Germany, 1999.
(12) Luther, K.; Oum, K.; Troe, J. *J. Phys. Chem. A* **2001**, *105*, 5535.
(13) Hahn, J.; Luther, K.; Troe, J. *Phys. Chem. Chem. Phys.* **2000**, *2*, 5098.
(14) Danis, F.; Caralp, F.; Veyret, B.; Loirat, H.; Lesclaux, R. *Int. J. Chem. Kinet.* **1989**, *21*, 715.
(15) Ellermann, T. *Chem. Phys. Lett.* **1992**, *189*, 175.
(16) Sullivan, J. H.; Davidson, N. *J. Chem. Phys.* **1951**, *19*, 143.
(17) Amphlett, J. C.; Whittle, E. *Trans. Faraday Soc.* **1968**, *64*, 2130.

(18) Tomkinson, D. M.; Pritchard, H. O. *J. Phys. Chem.* **1966**, *70*, 1579.
(19) Hippler, H.; Schubert, V.; Troe, J. *J. Chem. Phys.* **1984**, *81*, 3931.
(20) Hudgens, J. W.; Johnson, R. D., III.; Timonen, R. S.; Seetula, J. A.; Gutman, D. *J. Phys. Chem.* **1991**, *95*, 4400.
(21) FACSIMILE, AEA Technology, version 2, 1999.
(22) Huybrechts, G.; Narmon, M.; Mele, B. V. *Int. J. Chem. Kinet.* **1996**, *28*, 27.
(23) Matheson, I. A.; Sidebottom, H. W.; Tedder, J. M. *Int. J. Chem. Kinet.* **1974**, *6*, 493.
(24) DeMare, G. R.; Huybrechts, G. H. *Trans. Faraday Soc.* **1968**, *64*, 1311.
(25) Fenter, F. F.; Lightfoot, P. D.; Niiranen, J. T.; Gutman, D. *J. Phys. Chem.* **1993**, *97*, 5313.
(26) White, M. L.; Kuntz, R. R. *Int. J. Chem. Kinet.* **1971**, *3*, 127.
(27) Maergoiz, A. I.; Nikitin, E. E.; Troe, J.; Ushakov, V. G. *J. Chem. Phys.* **1998**, *108*, 5265.
(28) Maergoiz, A. I.; Nikitin, E. E.; Troe, J.; Ushakov, V. G. *J. Chem. Phys.* **1998**, *108*, 9987.
(29) Frisch, M. J.; Trucks, G. W.; Schlegel, H. B.; Scuseria, G. E.; Robb, M. A.; Cheeseman, J. R.; Zakrzewski, V. G.; Montgomery, J. A., Jr.; Stratmann, R. E.; Burant, J. C.; Dapprich, S.; Millam, J. M.; Daniels, A. D.; Kudin, K. N.; Strain, M. C.; Farkas, O.; Tomasi, J.; Barone, V.; Cossi, M.; Cammi, R.; Mennucci, B.; Pomelli, C.; Adamo, C.; Clifford, S.; Ochterski, J.; Petersson, G. A.; Ayala, P. Y.; Cui, Q.; Morokuma, K.; Malick, D. K.; Rabuck, A. D.; Raghavachari, K.; Foresman, J. B.; Cioslowski, J.; Ortiz, J. V.; Stefanov, B. B.; Liu, G.; Liashenko, A.; Piskorz, P.; Komaromi, I.; Gomperts, R.; Martin, R. L.; Fox, D. J.; Keith, T.; Al-Laham, M. A.; Peng, C. Y.; Nanayakkara, A.; Gonzalez, C.; Challacombe, M.; Gill, P. M. W.; Johnson, B. G.; Chen, W.; Wong, M. W.; Andres, J. L.; Head-Gordon, M.; Replogle, E. S.; Pople, J. A. *Gaussian 98*, revision A.7; Gaussian, Inc.: Pittsburgh, PA, 1998.
(30) Botschwina, P., private communication.
(31) Horn, M.; Botschwina, P. *Chem. Phys. Lett.* **1994**, *228*, 259.
(32) Maergoiz, A. I.; Nikitin, E. E.; Troe, J.; Ushakov, V. G. *J. Chem. Phys.* **1996**, *105*, 6277.
(33) Cobos, C. J.; Troe, J. *J. Chem. Phys.* **1985**, *83*, 1010.
(34) Pesa, M.; Pilling, M. J.; Robertson, S. H.; Wardlaw, D. M. *J. Phys. Chem. A* **1998**, *102*, 8526.
(35) Hippler, H.; Schubert, V.; Troe, J. *Ber. Bunsen−Ges. Phys. Chem.* **1985**, *89*, 760.
(36) Hirschfelder, J. O.; Curtiss, C. F.; Bird, R. B. *Molecular Theory of Gases and Liquids*; Wiley: New York, 1954.
(37) Reid, R. C.; Prausnitz, J. M.; Poling, B. J. *The Properties of Gases and Liquids*, 3rd ed.; McGraw-Hill: New York, 1987.
(38) Ruckenstein, E.; Liu, H. *Ind. Eng. Chem. Res.* **1997**, *36*, 3927.
(39) Liu, H.; Ruckenstein, E. *Ind. Eng. Chem. Res.* **1997**, *36*, 5488.
(40) Chen, S. H.; Davis, H. T.; Evans, D. F. *J. Chem. Phys.* **1982**, *77*, 2540.
(41) Chen, S. H. *Chem. Eng. Sci.* **1983**, *38*, 655.
(42) Karger, N.; Vardag, T.; Luedemann, H. D. *J. Chem. Phys.* **1990**, *93*, 3437.
(43) Eaton, A. P.; Akgerman, A. *Ind. Eng. Chem. Res.* **1997**, *36*, 923.
(44) Speedy, R. J.; Prielmeier, F. X.; Vardag, T.; Lang, E. W.; Luedemann, H. D. *Mol. Phys.* **1989**, *66*, 577.
(45) Terazima, M. *Acc. Chem. Res.* **2000**, *33*, 687.
(46) Green, N. J. B.; Spencer-Smith, R. D.; Rickerby, A. G. *Chem. Phys.* **1996**, *212*, 99.
(47) Troe, J. *Annu. Rev. Phys. Chem.* **1978**, *29*, 223.
(48) Bunker, D. L.; Davidson, N. *J. Am. Chem. Soc.* **1958**, *80*, 5090.
(49) Schwarzer, D.; Teubner, M. *J. Chem. Phys.* **2002**, *116*, 5680.
(50) Schwarzer, D.; Teubner, M., private communication.
(51) Saltiel, J.; Atwater, B. W. *Adv. Photochem.* **1988**, *14*, 1.
(52) Claridge, R. F. C.; Fischer, H. *J. Phys. Chem.* **1983**, *87*, 1960.
(53) Burnett, G. M.; North, A. M. *Transfer and Storage of Energy by Moleucles*; Vol. 1; Wiley: New York, 1969.
(54) Sceats, M. *Chem. Phys.* **1985**, *96*, 299.